arXiv:1608.03434v2 [cond-mat.mtrl-sci] 14 Sep 2016

Second-harmonic imaging microscopy for time-resolved investigations on transition metal dichalcogenides

J. E. Zimmermann,[1] G. Mette,[1,*] and U. Höfer[1]

[1] *Fachbereich Physik und Zentrum für Materialwissenschaften, Philipps-Universität, 35032 Marburg, Germany*

(Dated: September 15, 2016)

Abstract

Heterostructures of two-dimensional transition metal dichalcogenides (TMDC) have shown promise for various applications in optoelectronics and so-called valleytronics. Their operation and performance strongly depend on the stacking of individual layers. Here, optical second-harmonic generation (SHG) in imaging mode is shown to be a versatile tool for systematic time-resolved investigations of TMDC monolayers and heterostructures in consideration of the material's structure. Large sample areas can be probed in a single shot without the need of any mapping or scanning. By means of polarization dependent measurements, the crystalline orientation of monolayers or the stacking angles of heterostructures can be evaluated for the whole field of view. Pump-probe experiments then allow to correlate observed transient changes of the second harmonic response with the underlying structure. The corresponding time-resolution is virtually limited by the pulse duration of the used laser. As an example, polarization dependent and time-resolved measurements on single-layer MoS_2 and WS_2 flakes grown on a SiO_2 / Si(001) substrate are presented.

INTRODUCTION

Two-dimensional (2D) materials have been intensively investigated since the first successful isolation of graphene [1]. Recently, this interest has been stimulated further by the discovery of the special properties of single-layer transition metal dichalcogenides (TMDC) [2, 3]. Van-der-Waals coupled 2D materials now span the whole range from metallic over semiconducting up to isolating materials and their combination leads to fascinating opportunities for designing stacked heterostructures [4, 5].

TMDC heterostructures have shown promise for various electronic applications, in particular optoelectronic devices, such as pn-diodes [6–9], (field-effect) transitors [10–14], photovoltaic cells and photodetectors [8, 9, 15–17], light-emitting diodes [8, 9, 18] and nanolasers [19]. Moreover, future applications beyond conventional optoelectronics might be based on the coupled spin and valley physics of TMDC monolayers due to their broken inversion symmetry [20]. This coupling allows the excitation of specific spin carriers into a specific valley which has been demonstrated by optical pumping with circularly polarized light [21–24]. These findings pave the way for a new class of prospective devices called valleytronics.

The energy alignment of TMDC heterostructures [25–29] as well as interlayer charge- and energy-transfer processes [6, 30–34] are of particular interest in fundamental and applied research. Due to the Van-der-Waals coupling, arbitrary layer stacking is possible. Rotational misfit between two TMDC monolayers of a layered structure results in a corresponding rotation of the hexagonal Brillouin zones of the two layers leading to momentum-mismatched interlayer excitations. Therefore, the stacking influences charge and energy transfer and therby the performance of the device. It has been shown that the interlayer coupling of homo-stacked layers depends considerably on the respective stacking angles [35–38] and the same should hold for the coupling of hetero-bilayers [39–42]. Indeed, a distinct difference in the exciton dynamics of coherently and randomly stacked heterostructures has been observed [39]. However, most of the present time-resolved studies on TMDC heterostructures do not discuss the stacking of their materials at all. Furthermore, some studies report explicitly that their results do not depend on the relative orientation between the individual monolayers in the heterostructure [33, 43].

Thus, systematic studies are highly needed to investigate how structural characteristics

like the stacking angle of 2D heterostructures correlate with other physical properties of the materials such as the existence and dynamics of charge transfer excitons. In this work, we demonstrate that spatially resolved optical second-harmonic generation (SHG), i.e. SHG imaging microscopy, is a powerful experimental technique to perform such time-resolved studies in consideration of the material's structure. It allows to study systematically both the orientation and the charge carrier dynamics of TMDC monolayers and heterostructures with the same experimental setup. In particular, a complementary technique to analyze the stacking of the material is not needed. As an example, we report time-resolved SHG imaging microscopy studies on MoS_2 and WS_2 monolayer flakes grown by chemical vapor deposition (CVD) on a 300 nm SiO_2/Si(001) substrate.

TIME-RESOLVED SHG ON TMDCS

Previous studies already demonstrated that second harmonic generation is a versatile technique to investigate single- and multilayers of TMDCs [44–53]. It has been shown that the SH response of the TMDCs exhibits a dramatic odd-even oscillation with the number of layers consistent with the absence (presence) of inversion symmetry in odd (even) layers [44–47]. Rotational anisotropy SHG measurements probing the SH response of TMDC monolayers as a function of the crystal orientation reveal the expected six-fold rotational symmetry [45–47]. This allows the determination of crystallographic orientations for single-layer flakes [45–47], domain boundaries and orientations of CVD grown monolayer structures [47, 48, 50] as well as stacking angles of twisted bilayers [51].

Time-resolved SHG has also been applied to study the dynamics of various phenomena at surfaces and interfaces of bulk semiconductors. Its sensitivity to symmetry changes and to interface electronic states has been exploited for time-domain investigations of phase transformations [54, 55], of adsorbate reactions [56], of interface-specific electron dynamics [57–59] and to the detection of transient electric fields at interfaces [60–62]. One has to point out that the high sensitivity of SHG to the discussed quantities allows one to explore very small effects. For example, coverage changes on surfaces of less than 1% of a monolayer may be detected by means of SHG [56].

Time-resolved SHG experiments on TMDC samples have to cope with the small flake/domain size of exfoliated and CVD grown samples available at the moment. Therefore, almost all

previous optical experiments were performed at normal incidence by means of microscope objectives($\times 100$) with short working distances and probe beams focused to $\approx 1\,\mu$m. This kind of setup is disadvantageous for time-resolved pump-probe studies like SHG because it makes the non-collinear incidence of pump and probe beam difficult. As the pump beam also generates SH signal, this has to be differentiated from the SH response of the probe beam. Furthermore, the time-resolution is reduced by the dispersion of the used optical elements. These difficulties might explain why, to the best of our knowledge, there is only one published time-resolved SHG study on TMDCs. Here, the dynamical SH response of single-layer MoS_2 to intense above-bandgap photoexcitation was investigated [52].

SHG imaging microscopy combines the advantages of time-resolved SHG with an optical microscopy setup. The SH response of the sample is imaged optically magnified on a CCD chip. Similar setups have been used to study surface reactions like desorption or diffusion [63–65] as well as electric field distributions and carrier motion [66–69]. SHG imaging microscopy copes with both of the discussed challenges of time-resolved studies on TMDCs. On the one hand, the SH response of pump and probe beam can be separated very easily. On the other hand, the time-resolution is virtually limited by the pulse duration of the laser system. The SH response of large sample areas ($\approx 400 \times 400\,\mu\text{m}^2$) can be probed in a single shot without the need of any mapping or scanning. By means of polarization dependent measurements, the crystalline orientation of single-layer flakes and domains, or the stacking angles of heterostructures can be evaluated for the whole field of view. Pump-probe experiments at the corresponding area then allow to correlate observed transient changes of the SH response with the underlying structure. With this technique polarization- and time-resolved measurements can be performed systematically and routinely. SHG imaging microscopy is also suited to study fluence dependent phenomena [65].

EXPERIMENTAL PROCEDURE

The experiments were performed under ambient conditions using 40 fs laser pulses generated by a femtosecond Ti:Sapphire laser amplifier system (Coherent RegA) operating at 800 nm with a repetition rate of 100 kHz. The main part of the amplifier output (90 %) is used to pump a travelling-wave optical parametric amplifier (OPA) operating in the visible range. The output of the OPA is recompressed by a pair of LaFN28 Brewster prisms. This

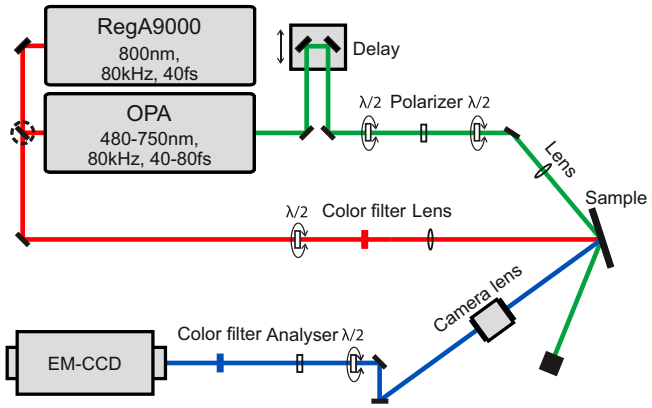

FIG. 1. (Color online) Experimental setup: fs-laser pulses are generated by a Ti:Sapphire laser amplifier system (RegA). The main part of the amplifier output (90 %) is used to pump an optical parametric amplifier (OPA) generating visible pump pulses. The remaining part of the amplifier output is used to probe the SH response. Pump and probe beam are focussed onto the sample under an angle of 50° and 18°, respectively. The specular reflected SH light of the probe pulse is imaged optically magnified by a camera lens on the CCD camera.

visible pump beam is then focussed under the angle of 50° onto the sample as illustrated in Fig.1. The remaining part of the amplifier output (10 %) is focused on the sample under an angle of 18° to probe the SH response. Due to the different incident angles the SH signals generated by the pump and the probe beam are spatially separated.

The specular reflected SH response of the probe beam is imaged optically magnified by a camera lens (Nikon Nikkor, 1 : 1.4 ED, $f = 50$ mm) on an electron-multiplied CCD chip (Princeton Instruments ProEM-HS) with a size of 1024×1024 pixels; each pixel covers an area of 13×13 μm^2 on the chip. The camera is sensitive in a spectral range from 300 nm up to 1050 nm and was operated in full image mode. The used magnification was M$\approx 35 - 40$, thus the visible sample region on the CCD was about $400 \times 400\,\mu$m^2. The overall resolution of our imaging microscopy setup is better than 4 μm as determined by a standard resolution target (c.f. Fig. S3 in the Supplemental Material (*SM*) [70]). Thus, the resolution is close to the diffraction limit of ≈ 2 μm.

The time-delay between pump and probe beam is varied by a motorized delay stage. The polarization of pump and probe beam can be varied by means of $\lambda/2$-plates. The polarization of the second-harmonic response is analyzed by a combination of $\lambda/2$-plate and

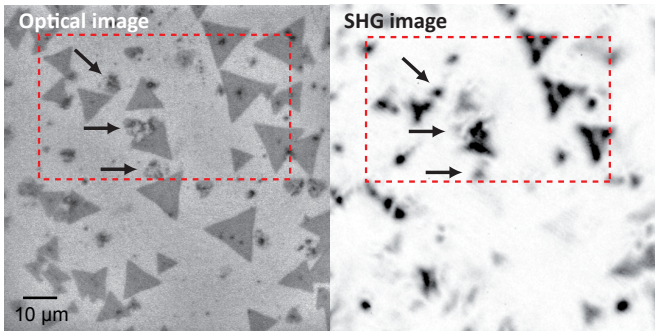

FIG. 2. Comparison of an optical image of the sample with the respective intensity-inverted SHG microscopy image ($100 \times 100\,\mu m^2$). Both images exhibit the MoS_2 flakes as dark triangular flakes while the more bulky WS_2 flakes (marked by arrows) show less contrast on the bright SiO_2/Si(001) substrate. The red box labels the region shown in Fig. 3.

analyzer. Color filters for separation of both the incident ω- and detected 2ω-light have been used (RG715, FBH400-40). The spot diameter of pump and probe beam on the sample [full width at half maximum (FWHM)] were 130 μm and 350 μm, respectively. A combination of $\lambda/2$-plate and polarizer enable the continuous variation of the incident pump fluences on the sample. The incident fluence of pump and probe beam was ≈ 0.3 mJ/cm^2 in each case. Long term measurements with these fluences applied did not exhibit any multishot damage.

The studied TMDC sample consists of MoS_2 and WS_2 monolayer flakes which were CVD grown successively on the same 300 nm SiO_2/Si(001) substrate (2D Semiconductors). Fig. 2 shows an optical microscope image ($\times 50$) in comparison to the respective SHG microscopy image (P-polarized SH component, $t_{\text{exposure}} = 300\ s$) which is intensity-inverted for better comparability. One can identify several dark triangular flakes and some additional bulky flakes showing less contrast on the bright SiO_2/Si(001) substrate. By means of photoluminescence measurements (not shown) the flakes have been identified as single-layer MoS_2 and WS_2, respectively.

RESULTS AND DISCUSSION

Polarization dependent measurements

Previous rotational anisotropy measurements probing the SH radiation component parallel (perpendicular) to the polarization of the fundamental field revealed the expected $\cos^2 3\theta$

($\sin^2 3\theta$) dependence [45–49]. Here, θ denotes the angle between the mirror plane in the crystal structure (i.e. the armchair direction) and the polarization of the probe beam. Rotating the sample then allows direct access to the symmetry of the sample and to the crystal orientation [45–49]. However, in order to exploit the advantage of SHG imaging microscopy probing a larger surface area at once, the sample is chosen to be fixed and the polarization of the fundamental is rotated. As it is known from literature [71] and further derived in the *SM* [70], the expected dependence of P- and S-polarized components of the SH intensity on the polarization yield

$$\mathbf{I}_{\mathrm{P}}^{2\omega}(\phi) \propto \cos^2(2\phi + 3\Psi) \tag{1}$$

$$\mathbf{I}_{\mathrm{S}}^{2\omega}(\phi) \propto \sin^2(2\phi + 3\Psi). \tag{2}$$

Here, ϕ denotes the angle of the polarization with respect to the horizontal and Ψ the angle between the armchair direction of the 2D-crystal and the horizontal as sketched in Fig. 3(b). Thus, instead of the six-fold rotational symmetry, a four-fold rotational symmetry is expected, but again the crystal orientation can be evaluated from the data. Please note, that because of the threefold rotational symmetry of the TMDC monolayers, SHG without phase information does not deduce opposite crystal orientations. Consequently, it only determines domain orientations modulo 60 °. Since the observed triangular MoS_2 flakes represent ideal orientation markers, the consistency of the evaluation can be checked easily (cf. Section 2 in the *SM* [70]).

A movie of the polarization dependent SHG microscopy measurements showing the P-polarized SH component ($t_{\mathrm{exposure}} = 60\ s$) for varying polarization of the fundamental from 0 ° to 180 ° in steps of 6 ° can be found in the *SM* [70]. Fig. 3 shows the corresponding polar plots of the SH intensity of some MoS_2 (c) and WS_2 (d) regions marked in the SHG microscopy image (a). As described above, the crystal orientations along the armchair direction of the three MoS_2 (WS_2) flakes are evaluated from the observed phase of the corresponding fits to 7 °, 16 °, and 2 ° (2 °, 9 °, and 16 °). A statistical analysis of 13 MoS_2 flakes finds that the orientations are distributed around $8.6° \pm 4.4°$ and $48.0° \pm 2.6°$ (c.f. Fig. S2 in the *SM* [70]). This indicates a predominant growth direction of MoS_2 most-likely induced by the geometry of the substrate. For WS_2, there were not enough monolayer flakes to perform a similar statistical analysis. Furthermore, one finds that the amplitudes of the rotational anisotropy for the WS_2 flakes differ strongly while the MoS_2 amplitudes are

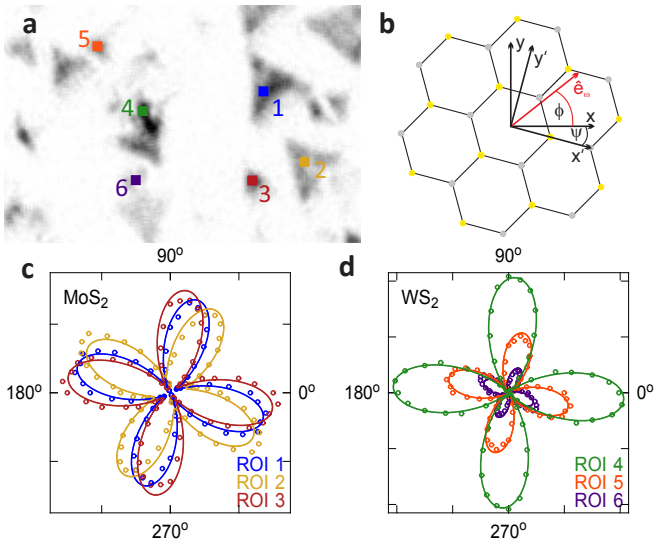

FIG. 3. (a) SHG microscopy image (P-polarized SH component, $t_{\text{exposure}} = 60\ s$) with colored regions of interests of the rotational anisotropy measurement. (b) Schematic drawing of the experimental geometry. (c/d) Polar plots of the P-polarized component of the SH intensity of MoS_2 and WS_2 flakes and corresponding fits (solid lines).

very similar. This indicates that the CVD growth conditions have led to much less uniform structures for the WS_2 flakes on the SiO_2/Si(001) substrate. This is in accordance with the observed bulky and inhomogeneous appearance of the WS_2 flakes in optical microscopy. While the performed photoluminescence measurements clearly suggest single-layered WS_2, one might suspect a partial existence of WS_2 multilayers.

One has to point out that the determination of the crystal orientation or stacking angles by means of SHG originates directly from the symmetry properties of the TMDC layers. Neither a complementary experimental technique nor further modelling is needed for the evaluation. This is in contrast to similar considerations for graphene which is, by the way, not accessible by SHG due to its inversion symmetry. Instead, the stacking of bilayer graphene has been studied systematically for example by the combination of structural and optical experimental techniques like transmission electron microscopy and Raman spectroscopy [72, 73].

Time-resolved measurements

The results of a time-resolved pump-probe experiment on the same surface area is shown in Fig. 4. The used pump-wavelength of 618 nm (2.01 eV) was chosen to match the energies

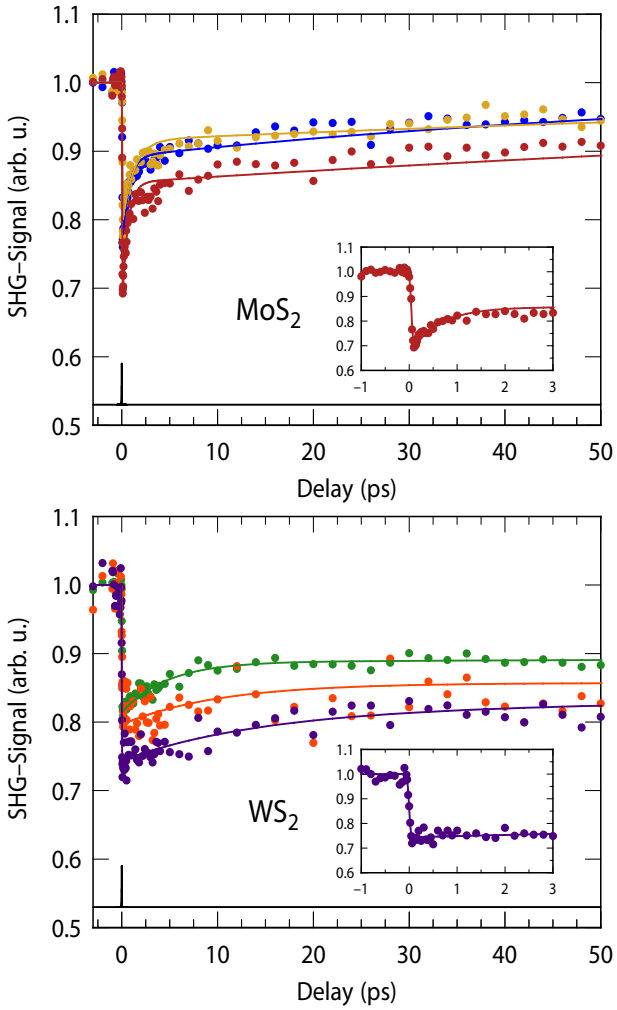

FIG. 4. Time-resolved SHG and corresponding fits obtained from MoS_2 (top) and WS_2 (bottom) flakes. The transients of both materials exhibit a fast pump-induced decrease of the SH response. The relaxation behavior differs considerably for the two materials. It can be described by means of a bi-exponential mechanism. The cross-correlation of pump and probe is indicated by the black line. The insets show the region close to temporal overlap. Coloring corresponds to Fig. 3.

of the A-exciton of WS_2 (1.95 eV) and the B-exciton of MoS_2 (2.01 eV) [33]. While the observed transients of the two different materials show a similar and fast pump-induced decrease of the SH response, their subsequent relaxation differs considerably, but can be described by a bi-exponential behavior in each case. The averaged time-constants obtained from the corresponding fits yield 840 ± 190 fs and 120 ± 26 ps for MoS_2 and 9 ± 3 ps and 2 ± 0.5 ns for WS_2.

We attribute the fast decrease of the SH response due to the pump-induced depopulation

of the valence band associated with the excitation of excitons. The subsequent progression then is interpreted as exciton relaxation within the monolayer materials. Since the MoS_2 values compare reasonably well with time-constants obtained from linear optical spectroscopy [31, 52, 74–80], this assignment seems appropriate. However, the overall number and values of reported time-constants differ quite strongly within these studies. Single- [52, 75, 79], bi- [31, 74, 76, 78, 80] and tri- [77] exponential behavior has been reported. The value of the shortest time-constant ranges from 500 fs up to 100 ps and that of the longest time-constant from 15 ps up to 500 ps. Similar variation holds for the reported studies on WS_2 [81–84]. These differences might be explained among other things by the use of different substrates, different temperatures, different pump- and probe energies and laser fluences, as well as varying sample quality, and of course, also by systematic effects of the applied techniques. Furthermore, a correlation of the crystal orientation and the pump laser polarization might be possible.

From this lack of clarity for these quite simple 2D monolayer systems, one might anticipate the complexity for 2D heterostructures and corresponding devices. Thus, systematic time-resolved studies on monolayer and heterostructure systems are mandatory in identifying the genuine physical effects and understanding the underlying mechanisms correlated to the layer stacking. Consequently, this knowledge will facilitate the further development and improvement of prospective applications based on 2D materials.

SUMMARY

The operation and performance of devices based on TMDC heterostructures strongly depend on the stacking of individual layers. Concurrently, reported results of time-resolved optical spectroscopy on simple TMDC monolayer systems reveal a large variability. We have introduced SHG imaging microscopy as a powerful method for the investigation of monolayers and heterostructures of two-dimensional transition metal dichalcogenides. In particular, it is suited to perform systematic pump-probe experiments and to correlate the observed transient changes of the second harmonic response to the stacking of the material. From polarization dependent measurements, the crystalline orientations of single-layer MoS_2 and WS_2 flakes grown on SiO_2 / Si(001) are evaluated. Time-resolved experiments exhibit a fast pump-induced decrease of the SH response in both materials while its relaxation

differs considerably for MoS_2 and WS_2. From the corresponding time-constants the transient changes are attributed to the excitation and relaxation of excitons within the monolayer materials.

ACKNOWLEDGEMENT

We thank J. Kuhnert and W. Heimbrodt for assistance with optical imaging and photoluminescence measurements. Funding by the Deutsche Forschungsgemeinschaft through SFB 1083 is gratefully acknowledged.

* gerson.mette@physik.uni-marburg.de

[1] K. S. Novoselov, A. K. Geim, S. V. Morozov, D. Jiang, Y. Zhang, S. V. Dubonos, I. V. Grigorieva, and A. A. Firsov, Science **306**, 666 (2004).

[2] K. F. Mak, C. Lee, J. Hone, J. Shan, and T. F. Heinz, Phys. Rev. Lett. **105**, 136805 (2010).

[3] A. Splendiani, L. Sun, Y. Zhang, T. Li, J. Kim, C.-Y. Chim, G. Galli, and F. Wang, Nano Lett. **10**, 1271 (2010).

[4] A. K. Geim and I. V. Grigorieva, Nature **499**, 419 (2013).

[5] H. Lim, S. I. Yoon, G. Kim, A. R. Jang, and H. S. Shin, Chem. Mater. **26**, 4891 (2014).

[6] C. H. Lee, G. H. Lee, A. M. van der Zande, W. C. Chen, Y. L. Li, M. Y. Han, X. Cui, G. Arefe, C. Nuckolls, T. F. Heinz, J. Guo, J. Hone, and P. Kim, Nat. Nanotechnol. **9**, 676 (2014).

[7] X. D. Duan, C. Wang, J. C. Shaw, R. Cheng, Y. Chen, H. L. Li, X. P. Wu, Y. Tang, Q. L. Zhang, A. L. Pan, J. H. Jiang, R. Q. Yu, Y. Huang, and X. F. Duan, Nat. Nanotechnol. **9**, 1024 (2014).

[8] A. Pospischil, M. M. Furchi, and T. Mueller, Nat. Nanotechnol. **9**, 257 (2014).

[9] B. W. H. Baugher, H. O. H. Churchill, Y. F. Yang, and P. Jarillo-Herrero, Nat. Nanotechnol. **9**, 262 (2014).

[10] B. Radisavljevic, A. Radenovic, J. Brivio, V. Giacometti, and A. Kis, Nat. Nanotechnol. **6**, 147 (2011).

[11] Z. Y. Yin, H. Li, H. Li, L. Jiang, Y. M. Shi, Y. H. Sun, G. Lu, Q. Zhang, X. D. Chen, and H. Zhang, ACS Nano **6**, 74 (2012).

[12] T. Georgiou, R. Jalil, B. D. Belle, L. Britnell, R. V. Gorbachev, S. V. Morozov, Y. J. Kim, A. Gholinia, S. J. Haigh, O. Makarovsky, L. Eaves, L. A. Ponomarenko, A. K. Geim, K. S. Novoselov, and A. Mishchenko, Nat. Nanotechnol. **8**, 100 (2013).

[13] T. Roy, M. Tosun, J. S. Kang, A. B. Sachid, S. B. Desai, M. Hettick, C. M. C. Hu, and A. Javey, ACS Nano **8**, 6259 (2014).

[14] C. J. Shih, Q. H. Wang, Y. Son, Z. Jin, D. Blankschtein, and M. S. Strano, ACS Nano **8**, 5790 (2014).

[15] L. Britnell, R. M. Ribeiro, A. Eckmann, R. Jalil, B. D. Belle, A. Mishchenko, Y. J. Kim, R. V. Gorbachev, T. Georgiou, S. V. Morozov, A. N. Grigorenko, A. K. Geim, C. Casiraghi, A. H. C. Neto, and K. S. Novoselov, Science **340**, 1311 (2013).

[16] W. J. Yu, Y. Liu, H. L. Zhou, A. X. Yin, Z. Li, Y. Huang, and X. F. Duan, Nat. Nanotechnol. **8**, 952 (2013).

[17] W. J. Zhang, C. P. Chuu, J. K. Huang, C. H. Chen, M. L. Tsai, Y. H. Chang, C. T. Liang, Y. Z. Chen, Y. L. Chueh, J. H. He, M. Y. Chou, and L. J. Li, Sci. Rep. **4**, 3826 (2014).

[18] J. S. Ross, P. Klement, A. M. Jones, N. J. Ghimire, J. Q. Yan, D. G. Mandrus, T. Taniguchi, K. Watanabe, K. Kitamura, W. Yao, D. H. Cobden, and X. D. Xu, Nat. Nanotechnol. **9**, 268 (2014).

[19] S. F. Wu, S. Buckley, J. R. Schaibley, L. F. Feng, J. Q. Yan, D. G. Mandrus, F. Hatami, W. Yao, J. Vuckovic, A. Majumdar, and X. D. Xu, Nature **520**, 69 (2015).

[20] D. Xiao, G. B. Liu, W. X. Feng, X. D. Xu, and W. Yao, Phys. Rev. Lett. **108**, 196802 (2012).

[21] K. F. Mak, K. L. He, J. Shan, and T. F. Heinz, Nat. Nanotechnol. **7**, 494 (2012).

[22] T. Cao, G. Wang, W. P. Han, H. Q. Ye, C. R. Zhu, J. R. Shi, Q. Niu, P. H. Tan, E. Wang, B. L. Liu, and J. Feng, Nat. Commun. **3**, 887 (2012).

[23] H. L. Zeng, J. F. Dai, W. Yao, D. Xiao, and X. D. Cui, Nat. Nanotechnol. **7**, 490 (2012).

[24] G. Sallen, L. Bouet, X. Marie, G. Wang, C. R. Zhu, W. P. Han, Y. Lu, P. H. Tan, T. Amand, B. L. Liu, and B. Urbaszek, Phys. Rev. B **86**, 081301 (2012).

[25] H. P. Komsa and A. V. Krasheninnikov, Phys. Rev. B **88**, 085318 (2013).

[26] J. Kang, S. Tongay, J. Zhou, J. B. Li, and J. Q. Wu, Appl. Phys. Lett. **102**, 012111 (2013).

[27] M. H. Chiu, C. D. Zhang, H. W. Shiu, C. P. Chuu, C. H. Chen, C. Y. S. Chang, C. H. Chen, M. Y. Chou, C. K. Shih, and L. J. Li, Nat. Commun. **6**, 7666 (2015).

[28] V. O. Özcelik, J. G. Azadani, C. Yang, S. J. Koester, and T. Low, Phys. Rev. B **94**, 035125 (2016).

[29] H. M. Hill, A. F. Rigosi, K. T. Rim, G. W. Flynn, and T. F. Heinz, Nano Lett. **16**, 4831 (2016).

[30] X. P. Hong, J. Kim, S. F. Shi, Y. Zhang, C. H. Jin, Y. H. Sun, S. Tongay, J. Q. Wu, Y. F. Zhang, and F. Wang, Nat. Nanotechnol. **9**, 682 (2014).

[31] F. Ceballos, M. Z. Bellus, H. Y. Chiu, and H. Zhao, ACS Nano **8**, 12717 (2014).

[32] P. Rivera, J. R. Schaibley, A. M. Jones, J. S. Ross, S. F. Wu, G. Aivazian, P. Klement, K. Seyler, G. Clark, N. J. Ghimire, J. Q. Yan, D. G. Mandrus, W. Yao, and X. D. Xu, Nat. Commun. **6**, 6242 (2015).

[33] A. F. Rigosi, H. M. Hill, Y. Li, A. Chernikov, and T. F. Heinz, Nano Lett. **15**, 5033–38 (2015).

[34] D. Kozawa, A. Carvalho, I. Verzhbitskiy, F. Giustiniano, Y. Miyauchi, S. Mouri, A. H. C. Neto, K. Matsuda, and G. Eda, Nano Lett. **16**, 4087 (2016).

[35] K. H. Liu, L. M. Zhang, T. Cao, C. H. Jin, D. A. Qiu, Q. Zhou, A. Zettl, P. D. Yang, S. G. Louie, and F. Wang, Nat. Commun. **5**, 4966 (2014).

[36] S. J. Zheng, L. F. Sun, X. H. Zhou, F. C. Liu, Z. Liu, Z. X. Shen, and H. J. Fan, Adv. Opt. Mater. **3**, 1600 (2015).

[37] R. Akashi, M. Ochi, S. Bordacs, R. Suzuki, Y. Tokura, Y. Iwasa, and R. Arita, Phys. Rev. Appl. **4**, 014002 (2015).

[38] P. C. Yeh, W. Jin, N. Zaki, J. Kunstmann, D. Chenet, G. Arefe, J. T. Sadowski, J. I. Dadap, P. Sutter, J. Hone, and R. M. Osgood, Nano Lett. **16**, 953 (2016).

[39] H. Heo, J. H. Sung, S. Cha, B. G. Jang, J. Y. Kim, G. Jin, D. Lee, J. H. Ahn, M. J. Lee, J. H. Shim, H. Choi, and M. H. Jo, Nat. Commun. **6**, 7372 (2015).

[40] H. Y. Yu, Y. Wang, Q. J. Tong, X. D. Xu, and W. Yao, Phys. Rev. Lett. **115**, 187002 (2015).

[41] W. C. Jin, P. C. Yeh, N. Zaki, D. T. Zhang, J. T. Liou, J. T. Sadowski, A. Barinov, M. Yablonskikh, J. I. Dadap, P. Sutter, I. P. Herman, and R. M. Osgood, Phys. Rev. B **91**, 121409 (2015).

[42] H. Wang, J. Bang, Y. Y. Sun, L. B. Liang, D. West, V. Meunier, and S. B. Zhang, Nat. Commun. **7**, 11504 (2016).

[43] K. Wang, B. Huang, M. Tian, F. Ceballos, M.-W. Lin, M. Mahjouri-Samani, A. Boulesbaa, A. A. Puretzky, C. M. Rouleau, M. Yoon, H. Zhao, K. Xiao, G. Duscher, and D. B. Geohegan, ACS Nano (2016), 10.1021/acsnano.6b01486.

[44] H. Zeng, G.-B. Liu, J. Dai, Y. Yan, B. Zhu, R. He, L. Xie, S. Xu, X. Chen, W. Yao, and X. Cui, Sci. Rep. **3**, 1608 (2013).

[45] Y. Li, Y. Rao, K. F. Mak, Y. You, S. Wang, C. R. Dean, and T. F. Heinz, Nano Lett. **13**, 3329 (2013).

[46] L. M. Malard, T. V. Alencar, A. P. M. Barboza, K. F. Mak, and A. M. de Paula, Phys. Rev. B **87**, 201401 (2013).

[47] N. Kumar, S. Najmaei, Q. Cui, F. Ceballos, P. M. Ajayan, J. Lou, and H. Zhao, Phys. Rev. B **87**, 161403 (2013).

[48] X.-Q. Zhang, C.-H. Lin, Y.-W. Tseng, K.-H. Huang, and Y.-H. Lee, Nano Lett. **15**, 410 (2015).

[49] Y. Miyauchi, R. Morishita, M. Tanaka, S. Ohno, G. Mizutani, and T. Suzuki, Jpn. J. Appl. Phys. **55**, 085801 (2016).

[50] X. Yin, Z. Ye, D. A. Chenet, Y. Ye, K. O'Brien, J. C. Hone, and X. Zhang, Science **344**, 488 (2014).

[51] W.-T. Hsu, Z.-A. Zhao, L.-J. Li, C.-H. Chen, M.-H. Chiu, P.-S. Chang, Y.-C. Chou, and W.-H. Chang, ACS Nano **8**, 2951 (2014).

[52] E. M. Mannebach, K.-A. N. Duerloo, L. A. Pellouchoud, M.-J. Sher, S. Nah, Y.-H. Kuo, Y. Yu, A. F. Marshall, L. Cao, E. J. Reed, and A. M. Lindenberg, ACS Nano **8**, 10734 (2014).

[53] G. Wang, X. Marie, I. Gerber, T. Amand, D. Lagarde, L. Bouet, M. Vidal, A. Balocchi, and B. Urbaszek, Phys. Rev. Lett. **114**, 097403 (2015).

[54] C. V. Shank, R. Yen, and C. Hirlimann, Phys. Rev. Lett. **51**, 900 (1983).

[55] H. W. K. Tom, G. D. Aumiller, and C. H. Brito-Cruz, Phys. Rev. Lett. **60**, 1438 (1988).

[56] U. Höfer, Appl. Phys. A-Mater. Sci. Process. **63**, 533 (1996).

[57] C. Voelkmann, M. Reichelt, T. Meier, S. W. Koch, and U. Höfer, Phys. Rev. Lett. **92**, 127405 (2004).

[58] M. Mauerer, I. L. Shumay, W. Berthold, and U. Hofer, Phys. Rev. B **73**, 245305 (2006).

[59] J. A. McGuire, M. B. Raschke, and Y. R. Shen, Phys. Rev. Lett. **96**, 087401 (2006).

[60] J. Qi, M. S. Yeganeh, I. Koltover, A. G. Yodh, and W. M. Theis, Phys. Rev. Lett. **71**, 633 (1993).

[61] G. Lupke, Surf. Sci. Rep. **35**, 77 (1999).

[62] W. A. Tisdale, K. J. Williams, B. A. Timp, D. J. Norris, E. S. Aydil, and X. Y. Zhu, Science **328**, 1543 (2010).

[63] G. T. Boyd, Y. R. Shen, and T. W. Hansch, Opt. Lett. **11**, 97 (1986).

[64] K. A. Schultz and E. G. Seebauer, J. Chem. Phys. **97**, 6958 (1992).

[65] K. Klass, G. Mette, J. Güdde, M. Dürr, and U. Höfer, Phys. Rev. B **83**, 125116 (2011).

[66] K. Wu, J. D. Canterbury, P. T. Wilson, and M. C. Downer, Phys. Stat. Sol. C **0**, 3081 (2003).

[67] T. Manaka, E. Lim, R. Tamura, and M. Iwamoto, Nat. Photonics **1**, 581 (2007).

[68] H. Satou, Y. Ohshima, H. Kohn, T. Manaka, and M. Iwamoto, J. Appl. Phys. **109**, 054506 (2011).

[69] J. D. Morris, T. L. Atallah, C. J. Lombardo, H. Park, A. Dodabalapur, and X. Y. Zhu, Appl. Phys. Lett. **102**, 033301 (2013).

[70] See Supplemental Material at [URL] for further experimental details .

[71] T. F. Heinz, M. M. T. Loy, and W. A. Thompson, Phys. Rev. Lett. **54**, 63 (1985).

[72] K. Kim, S. Coh, L. Z. Tan, W. Regan, J. M. Yuk, E. Chatterjee, M. F. Crommie, M. L. Cohen, S. G. Louie, and A. Zettl, Phys. Rev. Lett. **108**, 246103 (2012).

[73] R. W. Havener, H. L. Zhuang, L. Brown, R. G. Hennig, and J. Park, Nano Lett. **12**, 3162 (2012).

[74] T. Korn, S. Heydrich, M. Hirmer, J. Schmutzler, and C. Schüller, Appl. Phys. Lett. **99**, 102109 (2011).

[75] R. Wang, B. A. Ruzicka, N. Kumar, M. Z. Bellus, H. Y. Chiu, and H. Zhao, Phys. Rev. B **86**, 045406 (2012).

[76] Q. S. Wang, S. F. Ge, X. Li, J. Qiu, Y. X. Ji, J. Feng, and D. Sun, ACS Nano **7**, 11087 (2013).

[77] H. Shi, R. Yan, S. Bertolazzi, J. Brivio, B. Gao, A. Kis, D. Jena, H. G. Xing, and L. B. Huang, ACS Nano **7**, 1072 (2013).

[78] D. Z. Sun, Y. Rao, G. A. Reider, G. G. Chen, Y. M. You, L. Brezin, A. R. Harutyunyan, and T. F. Heinz, Nano Lett. **14**, 5625 (2014).

[79] M. Seo, H. Yamaguchi, A. D. Mohite, S. Boubanga-Tombet, J. C. Blancon, S. Najmaei, P. M. Ajayan, J. Lou, A. J. Taylor, and R. P. Prasankumar, Sci. Rep. **6**, 21601 (2016).

[80] S. Cha, J. H. Sung, S. Sim, J. Park, H. Heo, M. H. Jo, and H. Choi, Nat. Commun. **7**, 10768 (2016).

[81] J. Q. He, N. Kumar, M. Z. Bellus, H. Y. Chiu, D. W. He, Y. S. Wang, and H. Zhao, Nat. Commun. **5**, 5622 (2014).

[82] F. Ceballos, M. Z. Bellus, H. Y. Chiu, and H. Zhao, Nanoscale **7**, 17523 (2015).

[83] L. Yuan and L. B. Huang, Nanoscale **7**, 7402 (2015).

[84] R. Schmidt, G. Berghäuser, R. Schneider, M. Selig, P. Tonndorf, E. Malic, A. Knorr, S. M. de Vasconcellos, and R. Bratschitsch, Nano Lett. **16**, 2945 (2016).